Photocatalytic activity of TiO_2-WO_3 mixed oxides in formic acid oxidation

Francesca Riboni[a], Maria Vittoria Dozzi[a], Maria Cristina Paganini[b], Elio Giamello[b], Elena Selli[a,*]

[a] *Dipartimento di Chimica, Università degli Studi di Milano, Via Golgi 19, I-20133 Milano, Italy*

[b] *Dipartimento di Chimica, Università degli Studi di Torino, Via Giuria 7, I-10125 Torino, Italy*

A B S T R A C T

TiO_2 and Ti-W mixed oxide photocatalysts, with W/Ti molar ratios in the 0 – 5% range, were prepared through a simple sol-gel method, followed by annealing at 500 or 700 °C, and their photoactivity was tested in the photo-oxidation of formic acid in the aqueous phase under ambient aerobic conditions. XRPD analysis evidenced that in the presence of tungsten the anatase phase was stable even after calcination at 700 °C, with a progressively larger surface area and smaller particle dimensions with increasing tungsten content. Tungsten can both enter the titania lattice, as demonstrated by HAADF-STEM analysis, and also segregate as amorphous WO_3 on the photocatalysts surface, as suggested by XPS analysis. The best performing Ti/W oxide photocatalyst is that containing 1.0 mol% W/Ti, mainly due to the tungsten-induced stabilization effect of the anatase phase, whereas electron transfer from TiO_2 to WO_3, though compatible with the here performed EPR measurements, appears to have no beneficial effect in the investigated reaction, likely due to the low energy level of the conduction band of WO_3, from which electrons cannot efficiently transfer to adsorbed dioxygen.

Keywords: Photocatalysis; TiO_2; WO_3; formic acid oxidation; EPR analysis.

Corresponding author at: Dipartimento di Chimica, Università degli Studi di Milano, via Golgi 19, I-20133 Milano, Italy. Tel.: +39 02 503 14237; fax: +39 02 503 14300.

E-mail address: elena.selli@unimi.it (E. Selli)

1. Introduction

Photocatalysis represents a powerful tool to exploit the energy associated with light in a number of different applications, including pollutants removal from water and air for environmental remediation and solar into chemical energy conversion to produce so-called solar fuels. The key advantages of the use of TiO_2 as photocatalyst over other semiconductor oxides are well established and enormous efforts have been directed to improve its performance by reducing its intrinsic limitations. These mainly consist in the relatively large band gap (3.0 – 3.2 eV), that restricts the use of sunlight to promote photocatalytic reactions, in the low rate of electron transfer to reducible species and in the high rate of photoproduced electron-hole pairs recombination. The generation of long-living and spatially separated charge carriers thus appears a primary goal to be achieved. Combining TiO_2 with another semiconductor with suitable band gap and band edge values is one of the strategies so far explored for this aim [1-6].

In a composite photocatalytic system, consisting of two (or more [7]) semiconductor materials in intimate contact, the heterojunction formed at their interface generates a multicomponent structure which promotes the generation and mobility of the charge carriers, and thus improves the photocatalytic activity. Owing to the availability of a large number of semiconducting materials with different band gap and band offsets, the composition of a semiconductor composite can be conveniently designed to meet the energetic requirements of specific photocatalytic reactions. Among the many examples that can be found in the literature, Nb_2O_5/TiO_2 composites, featuring reduced rate of electron-hole recombination compared to pure TiO_2, have been investigated in the photocatalytic degradation of alcohols [8]. In combination with cerium oxide, TiO_2 has been shown to stabilize the Ce(III) oxidation state, which guarantees higher photoactivity of the CeO_x/TiO_2 composite materials. Indeed, Ce^{3+} centers and the concomitant formation of oxygen vacancies within the CeO_x/TiO_2 structure act as hole acceptors

and reduce the probability of electron-hole recombination [9]. TiO_2/WO_3 mixed oxides have been shown to exhibit higher photoactivity with respect to that of both single oxide components [3,5]. From the mechanistic point of view, the electrons photopromoted in the TiO_2 conduction band (CB) are expected to transfer to the CB of WO_3, while the holes remain more likely trapped in the valence band (VB) of titania. The so obtained spatial separation between electrons and holes would reduce their recombination probability, increase the electron lifetime and enhance the photoactivity performance of TiO_2/WO_3 mixed oxides [3,5].

In a recent study [6] some of us evidenced that Ti-W mixed oxide materials, prepared by a sol-gel synthesis starting from organic precursors and calcined at 700 °C, have a photocatalytic activity higher than that of pure titania prepared under identical conditions, in both an aqueous phase (formic acid degradation) and a gas phase (acetaldehyde decomposition) photocatalytic oxidation reaction. However the question remained open whether the beneficial effect on photoactivity of small amounts of tungsten should be associated to the presence of WO_3 domains within the TiO_2 structure, favoring the separation of photoproduced electron-hole couples, or to other tungsten-induced effects on the surface and bulk properties of titania.

Aiming at investigating more in depth the photoactivity vs. structure relationship of Ti-W oxide composite materials, in the present work we focus on the effects that different amounts of tungsten (W/Ti = 1 – 5 mol%) and different annealing temperatures (500 and 700 °C) have on the structure and photocatalytic activity of such materials. The photomineralization of formic acid (FA) in aqueous suspension, which was already investigated in our previous study [6] employing the photocatalysts series calcined at 700 °C, was employed as photoactivity test reaction. Photoactivity results are here interpreted in the light of the structural properties of the materials, as well as of the photogenerated charged species detected by EPR analysis.

2. Experimental

2.1. Photocatalysts preparation

Titanium(IV) isopropoxide ($Ti(OCH(CH_3)_2)_4$, Sigma-Aldrich, 97%) and tungsten(VI) hexa-ethoxide ($W(OC_2H_5)_6$, Alfa-Aesar, 99.8% (metal basis), 5 wt.% in ethanol) were used as titanium and tungsten precursors, respectively, for the synthesis of TiO_2-WO_3 mixed oxide photocatalysts, according to the already detailed procedure [6]. Briefly, anhydrous ethanol solutions were prepared containing the titanium and tungsten precursors in appropriate amount so as to produce mixed oxide samples with nominal W/Ti molar ratios equal to 1.0, 3.0 and 5.0%. Water was then added dropwise under vigorous stirring at 30 °C, so as to obtain a low-titanium-to-water molar ratio, favoring the formation of metal oxide nanoparticles [10]. The white slurry obtained after concentration under reduced pressure was kept in oven at 70 °C overnight and finally annealed either at 500 or at 700 °C under a 100 mL min^{-1} air flow for 4 h. Pure TiO_2 powders were synthesized and annealed under identical conditions, without adding the tungsten precursor. The samples were labeled TW*x*_*y*, with *x* referring to the W/Ti molar ratio (0 – 5%) and *y* to the annealing temperature in Celsius (500 or 700 °C).

2.2. Photocatalysts characterization

XRPD patterns were recorded with a Phillips PW3020 powder diffractometer, operating at 40 kV and 40 mA, using Cu Kα (λ = 1.54056 Å) as X-ray source. The diffractograms were recorded by continuous scanning in the 2θ-range = 20 – 80°, with a 0.05° step. Quantitative phase analysis was carried out with the Rietveld refinement method and the average crystallite size was determined by applying the Scherrer equation to the main anatase reflection (peak at 2θ = 25.5°, corresponding to the (1 0 1) crystal plane).

The BET surface area of each sample was determined by N_2 adsorption in a Micrometrics Tristar 3000 apparatus at liquid nitrogen temperature, after outgassing the samples at 300 °C for 4

h. The absorption properties of the powders were determined by means of a UV-visible reflectance spectrophotometer (Jasco, V-650), equipped with an integrating sphere. Ba_2SO_4 was adopted as reference material.

The High-Angle Annular Dark-Field Scanning Transmission Electron Microscopy (HAADF-STEM) images were recorded with an aberration-corrected HD-2700CS Hitachi STEM microscope, operated at an acceleration potential of 200 kV. A few drops of each powder suspended in ethanol were deposited on a perforated carbon foil, supported on a copper grid. After drying, the grid was mounted on the single tilt holder of the microscope.

Electron Paramagnetic Resonance (EPR) spectra were recorded by means of a Bruker EMX spectrometer with cylindrical cavity, operating at 100 kHz field modulation. Experiments were performed at liquid nitrogen temperature, either in the dark or under UV irradiation.

2.3. Photocatalytic activity tests

Formic acid (FA) photodegradation runs were performed under atmospheric conditions, as already described [11], employing a fixed photocatalyst amount (0.1 g L^{-1}) and a fixed initial FA concentration (1.0×10^{-3} mol L^{-1}). Prior to irradiation, the so-formed suspensions were left in the dark for 15 min under stirring, to attain adsorption equilibrium. The commercial lamp (Osram Powerstar HCI-T 150W/NDL) employed as irradiation source mainly emits visible light at wavelengths above 400 nm, with a small emission in the 350 – 400 nm range [11] and a full emission intensity on the photoreactor of 2.53×10^{-7} Einstein s^{-1} cm^{-2}. The residual amount of formate anion contained in the samples withdrawn from the photoreactor at different times was determined by ion chromatography with conductivity detection, after centrifugation. All photocatalytic runs were repeated at least twice to check their reproducibility.

3. Results and discussion

3.1. Crystal structure and physical properties

Fig. 1(a) shows the XRPD patterns of the materials. The TW*x*_500 photocatalysts proved to be composed of anatase phase, regardless of their W content (0 – 5 mol%). Conversely, among the samples annealed at 700 °C, pure TiO_2 (TW0_700) mainly consisted of rutile phase (90 wt.%), as revealed by the (1 1 0) reflection at 2θ = 27.4° appearing in its XRPD pattern, with a smaller contribution (10 wt.%) arising from anatase (2θ = 25.5°). However, all W-containing photocatalysts of the TW*x*_700 series were composed of pure anatase, demonstrating that the addition of small amounts of tungsten (in the 1 – 5 mol% range) during the synthesis completely inhibits the transformation of the anatase into the rutile phase, typically occurring when annealing TiO_2 at temperature above 600 °C [3,12].

As recently pointed out [13], in principle W^{6+} can be easily introduced in the titania lattice and substitute Ti^{4+} cations, due to their very similar ionic radii (ionic radius of W^{6+} = 0.0600 nm, ionic radius of Ti^{4+} = 0.0605 nm [14]). An accurate analysis of the main reflections of the anatase phase reveals that, regardless of the calcination temperature, the anatase reflection peak shifted toward lower 2θ-values with increasing tungsten content (Fig. 1(b)). This observation could be related to the expansion of the anatase cell occurring upon tungsten introduction and proves that a fraction of W can enter the TiO_2 lattice. Moreover, there is no evidence of crystalline phase corresponding to the formation of pure tungsten trioxide in the XRPD spectra of tungsten-containing photocatalysts. This indicates that tungsten oxide may be either amorphous or in concentration below the detection limit of XRPD analysis.

The size of anatase crystallites (d_A) in the samples, calculated by applying the Scherrer equation to the XRPD data, is reported in Table 1. While the anatase crystallite size in the TW*x*_500 photocatalyst series was found to be almost independent of the W content, being ca. 6

nm for all specimens, that calculated for pure titania TW0_500 was ca. double (13 nm). This is in line with the already reported tungsten ability of inhibiting the anatase crystallite growth [5]. Regarding the TW*x*_700 series, the anatase particle size in W-containing samples appear to slightly decrease with increasing W amount.

The specific surface area (SSA) values obtained from BET analysis perfectly match the trend of anatase nanoparticle sizes obtained from XRPD analysis. All W-containing samples of the TW*x*_500 series exhibit similar SSA, in line with their comparable nanoparticles size, while that of TW0_500 is significantly lower. The SSA values of samples annealed at 700 °C were markedly lower than those of samples calcined at 500 °C as a consequence of nanoparticles sintering, typically occurring upon annealing the oxide at higher temperature. Finally, the SSA values of the TW*x*_700 series are higher than that of pure TiO_2 (TW0_700) and monotonically increase as a function of the W/Ti molar ratio.

The absorption spectra of all photocatalysts are shown in Fig. 1(c). All powders exhibit an absorption onset at $\lambda \sim 400$ nm, owing to anatase TiO_2 band gap excitation. Only TW0_700 exhibits a red-shifted absorption threshold ($\lambda \sim 420$ nm), due to its high rutile-phase content. Moreover, as shown in the inset of Fig. 1(c), TW3_500 and TW5_500 exhibit slightly higher absorption around $\lambda \sim 450$ nm, compatible with the presence of WO_3 surface aggregates [15].

Tungsten incorporation within TiO_2 was confirmed by HAADF-STEM analysis. As shown in Fig. 2, the images of the TW*x*_500 (x = 1, 3 and 5) photocatalyst series highlight the presence of atomically dispersed tungsten, appearing as bright spots due to its Z-contrast in the titania lattice. The tiny light spots represent orderly aligned rows of W atoms incorporated into the TiO_2 matrix. Furthermore, the number of tungsten centers increases with increasing W/Ti nominal molar ratio, leading to a less spread W distribution in the case of TW5_500. A similar situation can be

assumed for the samples calcined at 700 °C. The average diameters of the TiO_2 crystallites obtained from STEM analysis are in agreement with those calculated from XRPD data (Table 1).

The chemical composition of both pure TiO_2 and TiO_2-WO_3 composite materials, annealed at either 500 or 700 °C, was investigated through X-ray photoelectron spectroscopy (XPS) in previous studies [6,16]. Apart from the Ti 2p features that confirmed the formation of a titania-based matrix also in TiO_2-WO_3 composite materials, the W $4f_{5/2}$ (BE ~ 37.5 eV) and W $4f_{7/2}$ (BE ~ 36 eV) signals also appeared in all the XPS spectra of tungsten-containing samples. These features are compatible with the formation of tungsten trioxide clusters, most likely on the surface of the composites [17]. The actual amount of W detected by XPS analysis increases with the W/Ti nominal molar ratio, W/Ti being 1.0 ± 0.1, 3.3 ± 0.2 and 5.3 ± 0.3 for TW1_500, TW3_500 and TW5_500 [16]. The main O 1s band was always found at BE ~ 530 eV, while the peak at BE ~ 533 eV corresponding to –OH groups on the oxide surface was almost negligible in the W-containing samples of the TW*x*_700 series [6], by virtue of the tungsten ability in reducing titania surface hydration.

3.2. Formic acid photocatalytic degradation

FA concentration decreased linearly with time under irradiation, as in previous studies [11,18]. Thus, the photocatalytic activity of all tested samples can be compared in terms of the zero order rate constants k (M s^{-1}) shown in Fig. 3, which were obtained by fitting the FA concentration vs. time linear decline occurring during the photocatalytic runs. Depending on the temperature of photocatalyst annealing, two photoactivity trends can be distinguished as a function of the W/Ti ratio. Indeed, for the TW*x*_500 photocatalysts series, k values decrease with increasing tungsten content; hence the most active material in this reaction is pure titania TW0_500. A similar photoactivity decrease with increasing tungsten content has been recently observed for the same photocatalytic reaction also with a series of TiO_2-WO_3 mixed oxide photocatalysts obtained by

coupling TiO_2 with different amounts of WO_3 according to an alkaline-catalyzed sol-gel method followed by an incipient wetting procedure [19].

Conversely, FA photodegradation proceeded at a higher rate with the W-containing photocatalysts of the TW*x*_700 series [6]. TW1_700 was the best performing photocatalyst and TW3_700 had an only slightly lower photoactivity, confirming that the presence of small amounts of tungsten has a beneficial effect on titania photoactivity [2,3]. This could be mainly related to the anatase composition of tungsten-containing samples and to their high crystallinity attained upon calcination at 700 °C, along with their larger surface area with respect to TW0_700, resulting from sintering inhibition [3] (see d_A values collected in Table 1). Among all Ti-W composite materials, independently of the calcination temperature, TW1_500 and TW1_700 exhibit the best performance in FA photo-oxidation, indicating W/Ti = 1 mol% as the optimum molar ratio for photocatalysts prepared under the here adopted conditions. Larger tungsten contents may result in a higher concentration of defect states available for charge carriers recombination, suppressing the rate of FA photodegradation.

Finally, if the photoactivity of Ti-W mixed oxides with the same nominal tungsten content are compared, those annealed at 700 °C, though having a much smaller SSA, generally proved to be better performing than those calcined at 500 °C. This effect, which is more evident for W/Ti = 3 and 5 mol%, very reasonably stems from the high crystallinity of anatase TW*x*_700 ensued through high temperature annealing.

3.3. Electron Paramagnetic Resonance analysis

EPR spectroscopy was used to investigate the fate of photo-promoted electrons, under UV irradiation and in the presence of O_2. The analysis was performed with two photocatalysts calcined at 500 °C, i.e. bare TiO_2 (TW0_500) and TW1_500, this latter exemplarily selected as

tungsten-containing sample. Fig. 4 shows the EPR signals detected with the two photocatalysts (panels (a) and (b), respectively) and their comparison (panel (c)).

The background EPR signal of pure TiO_2 corresponds to that of a nearly stoichiometric TiO_2 (Fig. 4(a), red trace). Upon UV irradiation (black trace), the typical feature corresponding to Ti^{3+} (g = 1.972) is observed due to the trapping of photopromoted electrons by the Ti^{4+} ions [20]. Furthermore, due to the presence of molecular oxygen, a fraction of photopromoted electrons is captured by O_2 and the EPR signals of the superoxide radical anion $O_2^{\bullet-}$ (g_{zz} = 2.034, g_{xx} = 2.003) consequently appear. In parallel, the photogenerated holes are trapped at oxygen sites and therefore become visible as O^- anions ($g_{\perp}$ = 2.027, $g_{\parallel}$ = 2.017) [21].

The background EPR spectrum of TW1_500 (Fig. 4(b), red trace) shows the presence of some nitric oxide (NO) trapped in closed cavities within the crystals and most likely ascribed to adventitious contamination. In the case of TW1_500 (Fig. 4(b), black trace), upon irradiation with UV light in the presence of O_2, the signals corresponding to oxygen-based paramagnetic species ($O_2^{\bullet-}$ and O^- with the same g values observed for bare titanium dioxide, see above) are observed. The comparison between the EPR spectra of TW0_500 and TW1_500, both recorded under UV irradiation and in O_2 atmosphere (Fig. 4(c)), highlights that in the mixed oxide the EPR signals of all species generated by charge carriers trapping (Ti^{3+}, $O_2^{\bullet-}$ and O^-) are less intense than those observed for pure titania.

Photoproduced electron-hole couples, once generated, can either recombine, be trapped in the bulk or react with species adsorbed on the surface of the semiconductor nanoparticles [22]. In pure titania, in the absence of molecular oxygen, photopromoted electrons are partly trapped in TiO_2, as corroborated by the presence of the EPR signal due to paramagnetic Ti^{3+} [5,23,24]. However, the electron trapping ability of the oxide is reduced in the presence of O_2, which is able to scavenge electrons, as proved by the generation of oxygen species, such as $O_2^{\bullet-}$ and H_2O_2. In

addition, EPR experiments performed by Zhao et al. with irradiated TiO_2-WO_3 under anaerobic conditions [5] indicate that the majority of photopromoted electrons are transferred to WO_3. Thus, the lower intensity of the EPR signals obtained with TW1_500 might be a consequence of either a less effective charge carriers trapping in this sample with respect to TW0_500, or an effective electron transfer from Ti^{3+} to W^{5+}. Direct evidence of W^{5+} formation might have been provided only by EPR measurements at very low temperature.

3.4. Photocatalytic activity vs. structural features of the Ti-W mixed oxides

HAADF-STEM images (Fig. 2) provide evidence that W^{6+} cations are introduced within the hosting TiO_2 lattice, while previously reported XPS characterization [16] indicate that WO_x aggregates can be present on the Ti-W mixed oxide surface. Thus, photopromoted electrons may produce W^{5+} species [5], either within the W-doped titania lattice, or by electron transfer from TiO_2 to WO_3 domains on the photocatalyst surface, triggered by the lower CB of WO_3 with respect to that of titania (*i.e.*, CB (TiO_2) ~ –0.1 V and CB(WO_3) ~ 0.4 V, both referred to SHE) [25].

Upon irradiation under aerobic conditions, EPR spectra proved that in the Ti-W mixed oxides both Ti^{3+} and $O_2^{\bullet-}$ paramagnetic species were present in smaller amount than in pure titania. This finding suggests that, during FA photo-oxidation reactions, photopromoted electrons may either be trapped at W^{5+} sites or be transferred to surface WO_3 aggregates. However, if this occurs, their subsequent transfer to adsorbed dioxygen would be inhibited [19] and an increased electron-hole recombination would result, with a consequently decreased efficiency in FA photocatalytic oxidation, this reaction notoriously proceeding through direct combination of the organic substrate with VB holes [26]. In fact, all Ti-W mixed oxides annealed at 500 °C were less active than pure titania in FA photo-oxidation (Fig. 3, left panel). In contrast, the better performance in FA photo-oxidation of the Ti-W mixed oxides annealed at 700 °C with respect to TW0_700 (Fig.

3, right panel) should mainly be ascribed to their highly crystalline anatase composition and to their higher SSA. In particular, the presence of tungsten led to a decrease in the anatase particle size with a consequent increase in the SSA of the mixed oxide photocatalysts (Table 1). Higher SSA values together with higher anatase content and crystallinity are often reported to play a remarkable role in enhancing the rate of heterogeneous photocatalytic reactions [4].

Tungsten addition may also generate a composite structure in TiO_2 that promotes the electron transfer from excited TiO_2 to WO_3, which in the here investigated W-containing photocatalyst are expected to reside mainly on the W-doped TiO_2 surface [16]. However this would produce a decrease in photoactivity in the here investigated reaction due to the lower energy level of the WO_3 CB band, from which electrons cannot efficiently transfer to O_2 in FA oxidation.

Furthermore, the introduction of a W excess into the titania lattice might increase the number of electron-hole recombination centers, which negatively affects the photoactivity of the materials. Under present conditions, W/Ti > 1 mol% proved to be negative for the photocatalysts performance (Fig. 3). The best performing Ti-W mixed oxide photocatalysts, calcined at 500 or 700 °C, were those containing the lowest amount of tungsten. This implies that titania-based mixed oxide photocatalysts with a lattice cell similar to that of anatase TiO_2 (see Fig. 1(b)) ensured the highest photoactivity in the investigated reaction.

4. Conclusions

Ti-W oxide composite photocatalysts annealed at 700 °C proved more effective than pure TiO_2 in promoting FA photodegradation, essentially due to the beneficial physico-chemical properties ensued by W addition in the TiO_2 lattice, i.e. anatase composition due to its retarded transformation into the rutile phase, enhanced surface area, higher crystallinity. On the other hand, Ti-W mixed oxides photocatalysts annealed at 500 °C were less efficient in FA photocatalytic oxidation with respect to pure titania TW0_500. In fact, if electron transfer from

TiO_2 to surface tungsten oxide aggregates occurs in these materials, it would result in lower photoactivity due to the hampered transfer of photopromoted electrons from the photocatalyst to dioxygen. Ti/W = 1 mol% was identified as the optimum mixing ratio, which guarantees minimal distortion of TiO_2 lattice parameters, low concentration of structure defects, anatase phase stabilization even upon calcination at 700 °C, and best photoactivity within the here investigated Ti-W mixed oxides.

Acknowledgements

This work received support from the Cariplo Foundation through the 2013-0615 grant to the project *Novel Photocatalytic Materials based on Heterojunctions for Solar Energy Conversion*. We thank professor Jeroen van Bokhoven for the permission to reproduce the HAADF-STEM images which were recorded at ETH Zurich.

References

[1] M. Dahl, Y. Liu, Y. Yin, *Chem. Rev.* 114 (2014) 9853–9889.

[2] X.Z. Li, F.B. Li, C.L. Yang, W.K. Ge, J. Photochem. Photobiol. A: Chem. 141 (2001) 209–217.

[3] K.K. Akurati, A. Vital, J.P. Dellemann, K. Michalow, T. Graule, D. Ferri, A. Baiker, Appl. Catal. B Environ. 79 (2008) 53–62.

[4] B. Tryba, M. Piszcz, A.W. Morawski, Intern. J. Photoen. (2009) 297319.

[5] D. Zhao, C. Chen, C. Yu, W. Ma, J. Zhao, J. Phys. Chem. C 113 (2009) 13160–13165.

[6] F. Riboni, L.G. Bettini, D.W. Bahnemann, E. Selli, Catal. Today 209 (2013) 28–34.

[7] H. Kim, J. Kim, W. Kim, W. Choi, J. Phys. Chem. C 115 (2011) 9797–9805.

[8] T. Ohuchi, T. Miyatake, Y. Hitomi, T. Tanaka, Catal. Today 120 (2007) 233–239.

[9] H. Yang, K. Zhang, R. Shi, A. Tang, J. Am. Ceram. Soc. 90 (2007) 1370–1374.

[10] G. Oskam, A. Nellore, R.L. Penn, P.C. Searson, J. Phys. Chem. B 107 (2003) 1734–1738.

[11] M.V. Dozzi, L. Prati, P. Canton, E. Selli, Phys. Chem. Chem. Phys. 11 (2009) 7171–7180.

[12] N. Couselo, F.S.García Einschlag, R.J. Candal, M. Jobbágy, J. Phys. Chem. C 112 (2008) 1094–1100.

[13] A.M. Cant, F. Huang, X.L. Zhang, Y. Chen, Y.B. Cheng, R. Amal, Nanoscale 6 (2014) 3875–3880.

[14] R.D. Shannon, Acta Cryst. A 32 (1976) 751–767.

[15] P.P. González-Borrero, F. Sato, A.N. Medina, M.L. Baesso, A.C. Bento, G. Baldissera, C. Persson, G.A. Niklasson, C.G. Granqvist, A. Ferreira Da Silva, Appl. Phys. Lett. 96 (2010) 061909.

[16] M. Carrus, F. Riboni, M. Fantauzzi, A. Rossi, E. Selli, J. van Bokhoven, Appl. Catal. A Gen. 519 (2016) 130–138.

[17] G. Orsini, V. Tricoli, J. Mater. Chem. 21 (2011) 14530–14542.

[18] C. Bernardini, G. Cappelletti, M.V. Dozzi, E. Selli, J. Photochem. Photobiol. A Chem. 211 (2010) 185–192.

[19] M.V. Dozzi, S. Marzorati, M. Longhi, M. Coduri, L. Artiglia, E. Selli, Appl. Catal. B Environ. 185 (2016) 157–165.

[20] S.K. Lee, P.K.J. Robertson, A. Mills, D. McStay, N. Elliott, D. McPhail, Appl. Catal. B Environ. 44 (2003) 173–184.

[21] G. Panarelli, S. Livraghi, S. Maurelli, V. Poliotto, M. Chiesa, E. Giamello, J. Photochem. Photobiol. A Chem. 322–323 (2016) 27–34.

[22] A.L. Linsebigler, G. Lu, J.T. Yates Jr, Chem. Rev. 95 (1995), 735–758.

[23] M. Chiesa, M.C. Paganini, S. Livraghi, E. Giamello, Phys. Chem. Chem. Phys. 15 (2013) 9435–9447.

[24] S. Tatsuma, S. Saitoh, P. Ngaotrakanwiwat, Y. Ohko, A. Fujishima, Langmuir 18 (2002) 7777–7779.

[25] D.E. Scaife, Sol. Energy 25 (1980) 41–54.

[26] H. Park, W. Choi, J. Phys. Chem. B 108 (2004) 4086–4093.

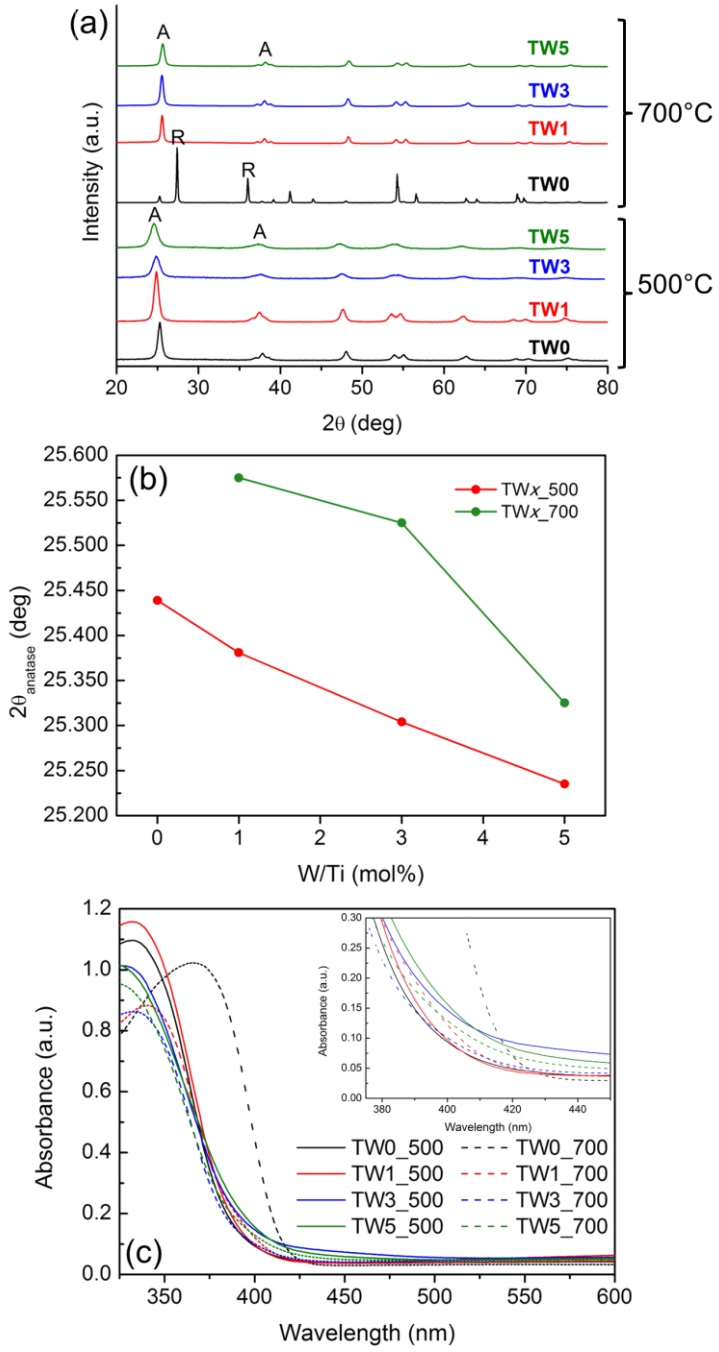

Fig. 1. (a) XRPD patterns of pure TiO_2 and of all W-containing samples, calcined at either 500 °C (bottom) or 700 °C (top), these latter taken from ref. [6]. A and R indicate the main anatase and rutile reflections, respectively. (b) Dependence of the 2 θ-value of the main anatase reflection (*i.e.*, 2 θ ~ 25.5°) on the W content in all samples. (c) UV-vis absorbance of all the synthesized TW*x* samples, either annealed at 500 °C (full lines) or 700 °C (dashed lines).

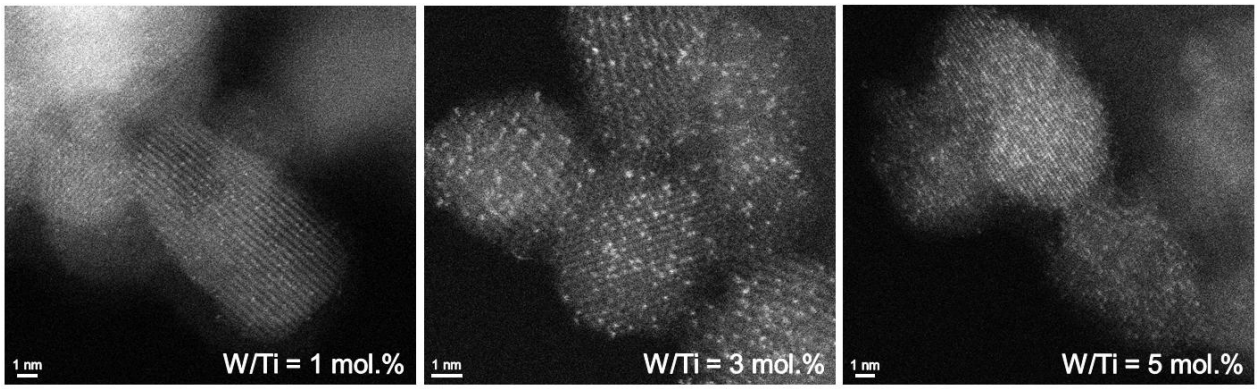

Fig. 2. HAADF-STEM images of TW1_500, TW3_500 and TW5_500 (from left to right).

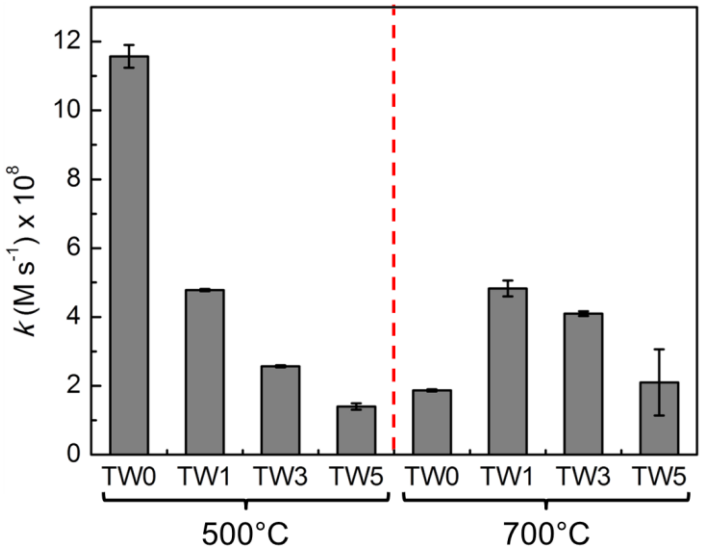

Fig. 3. Zero-order rate constant of formic acid degradation (*k*), obtained with the TW*x*_500 (left) and TW*x*_700 (right) photocatalysts.

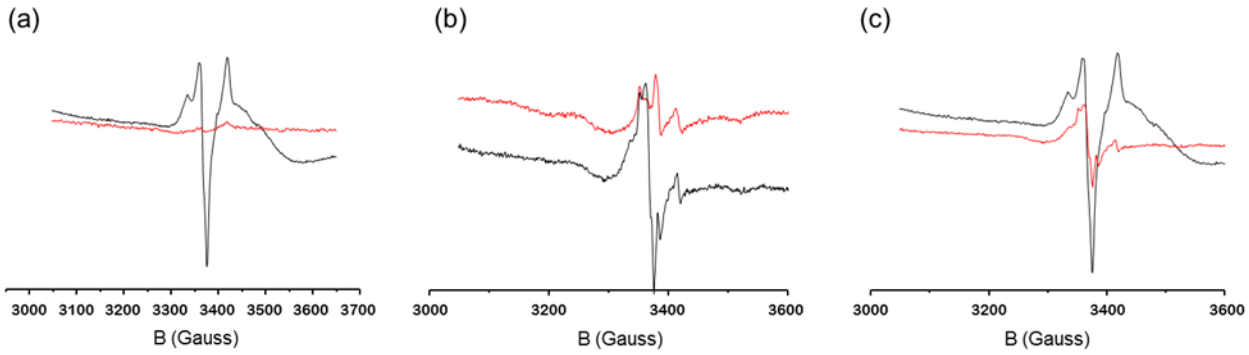

Fig. 4. EPR spectra of (a) TW0_500, as it is (red trace) and under UV irradiation in O_2-atmosphere (black trace); (b) TW1_500, as it is (red trace) and under UV irradiation in O_2-atmosphere (black trace). (c) Comparison between the EPR spectra of TW0_500 and TW1_500 (black and red traces, respectively), both under UV irradiation in O_2-atmosphere.

Table 1

Anatase particles dimension, d_A, obtained from XRD analysis assuming the absence of amorphous material and specific surface area, SSA, obtained from BET analysis of the synthesized TiO_2 and Ti-W mixed oxide materials.[a]

Sample	d_A (nm)	SSA (m^2 g^{-1})
TW0_500	13	44.6
TW1_500	6	206
TW3_500	5	202
TW5_500	6	198
TW0_700[b]	39	6.7
TW1_700	24	14.8
TW3_700	20	28.7
TW5_700	15	52.9

[a] All values reported for the TW*x*_700 series are taken from ref. [6].

[b] This sample mainly consists of rutile, its anatase content being ca. 10%.